

# Nonlinear Analysis of the Lightcurve of the Variable Star R Scuti

J. R. Buchler @1\*, Z. Kolláth @1\*\*, T. Serre, @1 & J. Mattei @2

@1 Physics Department, University of Florida, Gainesville, FL 32611 @2 AAVSO, Cambridge, MA 02138

30 september

**Abstract.** It is first shown that the observational light curve data of R Scuti, a star of the RV Tau type, is not multi-periodic, and that it cannot have been generated by a linear stochastic (AR) process. By default, the signal must be a manifestation of deterministic chaos. We use a novel nonlinear time-series analysis, the global flow reconstruction technique, to probe the properties of the irregular pulsation cycles. We show in particular that the chaotic dynamics of this star's complicated lightcurve is captured by a simple 4D polynomial map or flow (4 first order ODEs).

Importantly also, the method allows us to *quantify* an irregular signal which has the potential benefit for extracting novel stellar constraints from an irregular light-curve.

Finally, from the low dimensionality 4 of the flow we can infer a simple physical picture of the pulsations, and arguments are presented that the pulsations of R Sct are the result of the nonlinear interaction of two vibrational normal modes of the star.

**Key words:** Not yet given.

## 1. INTRODUCTION

It has been known for a long time that the metal-poor, Population II Cepheids, labelled W Virginis and RV Tauri stars, often pulsate irregularly (*e.g.* Ludendorff 1928; Kukarkin 1975). In fact, the pulsations of the W Vir stars which are of lower period and lower luminosity, are essentially regular (periodic), but as the periods increase alternations appear in the oscillations which however remain small for the W Vir stars, *i.e.* up to about 35 days (*e.g.* Arp 1955). At still higher periods, *i.e.* in the RV Tau

regime, the pulsations become more irregular, with alternating very deep and shallow minima and with large, long-term modulations in the amplitude.

The little theoretical work on these stars has been confined to their evolution. They are believed to be low mass, typically  $0.6 - 0.8M_{\odot}$  which, after helium exhaustion in the core, evolve to the red to the second giant branch and then enter the instability strip (Gingold 1974). Essentially no theoretical attention had been paid to their pulsations because of the want of a credible mechanism for the irregularity. Some eight years ago the numerical hydrodynamical *modelling* of W Vir stars of Buchler & Kovács (1987, hereafter BK87; see also Kovács & Buchler 1988, hereafter KB88; reviewed in Buchler 1990) showed that the irregularity in the pulsations is the manifestation of *low-dimensional chaos* and that it is no longer necessary to invoke a *deus ex machina*, such as, for example, postulated irregular convective phenomena. (We recall that chaos occurred in the purely radiative hydro-models.) Unfortunately, at the time, it was not possible to support these theoretical conclusions as to the chaotic nature of the pulsations with an analysis of *observational data*. The primary reasons were the lack of suitable methods of analysis, on the one hand, and of suitable observational data sets, on the other hand. However, in the last decade a great deal of progress has been made in nonlinear time-series analysis.

Seemingly erratic data can have a strong deterministic component in addition to a stochastic or noisy background. The goal of nonlinear signal processing is to detect the presence of such a deterministic signal, and to infer information about the dynamics that generates it, most often without *any a priori* knowledge thereof. Such a feat is possible if the dynamics is sufficiently low-dimensional which means that the signal is generated by a flow or a map with only a few variables. One can then hope to make a connection between these variables and corresponding physical variables, and to obtain a physical understanding of the pulsational behavior. We refer the reader to some recent reviews, *e.g.* Weigend & Gershenfeld (1994), here-

\* e-mail address: buchler@phys.ufl.edu

\*\* on leave from Konkoly Observatory, Budapest, Hungary

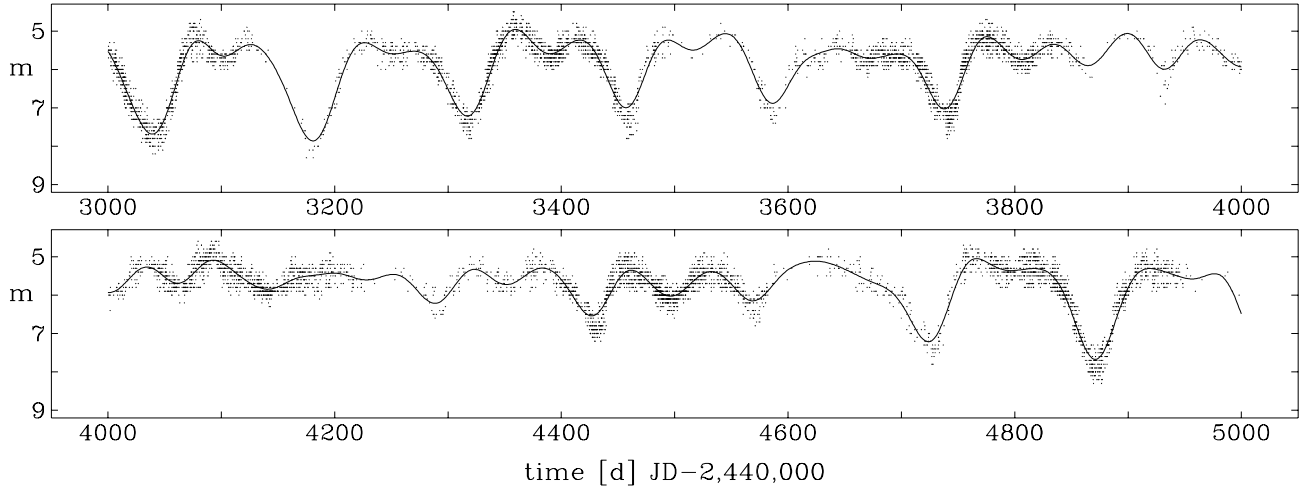


**Fig. 1.** Typical observed light curve segments for R Scuti. *Dots*: the individual observations, *line*: the smoothed filtered signal.

after WG94; Abarbanel *et al.* (1993), hereafter ABST93; Casdagli *et al.* (1992).

In astronomical observations we are usually limited to measuring a *single variable*, namely the magnitude (and perhaps, the radial velocity). Fortunately a very powerful tool has emerged from nonlinear science in the form of embedding theorems. Quite generally, in order to obtain information about the dynamics it is not necessary to measure *all* the phase-space variables, but it is sufficient to know the temporal behavior of *one* of them. In fact, it is enough to know the behavior of a single variable which is a function of the phase-space variables, such as the luminosity or the radial velocity. To apply the theorems to an observational time-series it is necessary however to sample the phenomenon at equally spaced time-intervals. While this is easy to do under the controlled conditions of a laboratory experiment, in long-term astronomical observations it is essentially impossible, whether because of telescope scheduling constraints and politics, sky obscuration or other causes.

Nonlinear techniques are new in Astronomy, and, quite generally, most astronomical observations have not been made with a nonlinear analysis in mind. As a consequence the measured light-curve data are often not suitable for the modern tools of analysis. Rarely are enough pulsation cycles covered by the observations to provide a 'typical' sample. The sampling rate, *i.e.* the number of points per cycle, is often too small. Large, and even regular gaps in the data pose no problem (in contrast to the standard aliasing problems in linear Fourier analyses), but data segments that are too short can make an analysis impossible. Finally, the signal to noise ratio is often too small.

Recently, the American Association of Variable Star Observers (AAVSO) has completed a compilation of the observational data on some RV Tau type stars. Of these

the R Scuti light-curve is particularly long (last 31 years) and relatively well sampled. Furthermore this star has a large pulsational amplitude, making the observational errors relatively small. We have taken advantage of the availability of the AAVSO data, and of the power of the global flow reconstruction method (Serre, Kolláth & Buchler 1995a, hereafter SKB), to analyze its pulsations.

In order to establish the reliability of the global flow reconstruction method we have presented extensive tests in SKB. These tests were performed on the well studied known Rössler attractor which consists of 3 ODEs (*cf.* also Brown 1992). Noise was also added to the Rössler data in order to simulate a more realistic astronomical environment. Our reason for choosing the Rössler attractor for benchmark tests is that, superficially at least, it bears a strong resemblance to the attractor that has been found in the pulsations of W Vir models (BK87; KB88). In SKB it is shown that from the mere knowledge of a relatively *short* stretch of the temporal behavior of *only one* of the Rössler variables the global flow reconstruction technique correctly recovers (a) the dimension of 3 for the Rössler system, and (b) the Lyapunov exponents and fractal dimension of the attractor. (We note that for such short a data set a computation of the correlation dimension would not be able to come up with a good estimation of the fractal dimension, and would not give any information about number of ODEs that generate the Rössler band).

We have also applied the global flow reconstruction technique to the analysis of the pulsations of one of these W Vir models. This numerical hydrodynamical study which discretized the star into 60 mass shells thus corresponded to the solution of 180 nonlinear coupled first order ODEs (180D space). The flow reconstruction shows that the W Vir model pulsations are found to be generated by a mere 3 dimensional flow. The reader may appreciate

that this dimensional shrinkage from 180 to 3 is nontrivial, neither mathematically nor physically. The physical implications of this result are discussed in Serre *et al.* (1995b).

In a Letter (Buchler, Serre, Kolláth, & Mattei 1995, hereafter BSKM) we have already described the highlights of our analysis of the lightcurve of R Sct. Here we provide not only a more thorough description of the tests that lead to that conclusion, but we also present additional tests. Furthermore, we discuss the physical implications of this result. In a companion paper (Kolláth, Buchler, Serre & Mattei 1995) we will communicate the analysis of AC Herculis, another star of the same type.

In §2 we discuss the data preparation procedure. In §3 we present two standard astronomical analyses, *viz.* a multi-periodic Fourier decomposition and an autoregressive (AR) scheme, respectively. We show that neither are compatible with the observational data. In §4 we present the results of the global flow reconstruction of the R Sct data followed by a discussion in §5. A physical picture of the uncovered low dimensionality of the dynamics is given in §6. In §7 we conclude with an evaluation of the global reconstruction method and its prospects for Astronomy.

## 2. THE DATA PREPARATION

An important problem arises in connection with the separation of the measured data into 'signal' and 'noise'. In order to extract information about the dynamics which generates the light-curve, it is clear that one wants to eliminate as much as possible observational noise, as well as noise that is extraneous to the star. Even then, however, there generally will still be a remaining 'noise' that has its origin in convection and turbulence, and which, strictly speaking, is part of the dynamics. It is well known that turbulent motions are usually very *high*-dimensional behavior (they involve many modes), and this therefore would seem to defeat *a priori* the purpose and any attempt to uncover any *low*-dimensional behavior, unless the pulsation can be separated into a large amplitude, low-dimensional 'true' pulsation and a low amplitude, but high-dimensional jitter. The success of our analysis seems to indicate that in the case of the pulsating stars of interest to us here, such a separation is indeed possible and that the high-dimensional jitter can be eliminated together with the true noise, leaving the low-dimensional signal relatively undisturbed.

The smoothing and filtering of the data is therefore an important and delicate part of any analysis of 'real' data. Here, too little smoothing will not suppress the high-dimensional component and preclude a successful search for low-dimensional behavior. On the other hand too much smoothing can severely distort or even destroy the low-dimensional component. Furthermore, certain types of filtering (IFR) can increase the embedding dimension (but not reduce it!, *q.v.* ABST93).

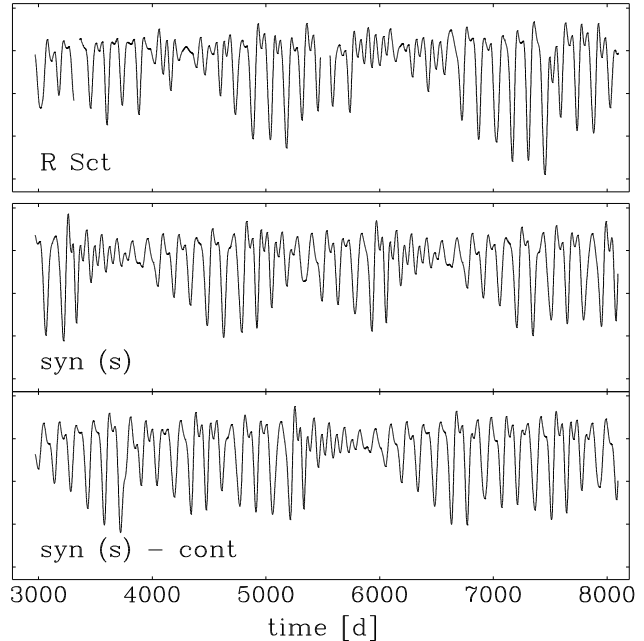


**Fig. 2.** *Top:* The smoothed light curve of R Scuti, Julian Day 2,438,000+; *s* data set. *Below:* two segments of the same synthetic signal.

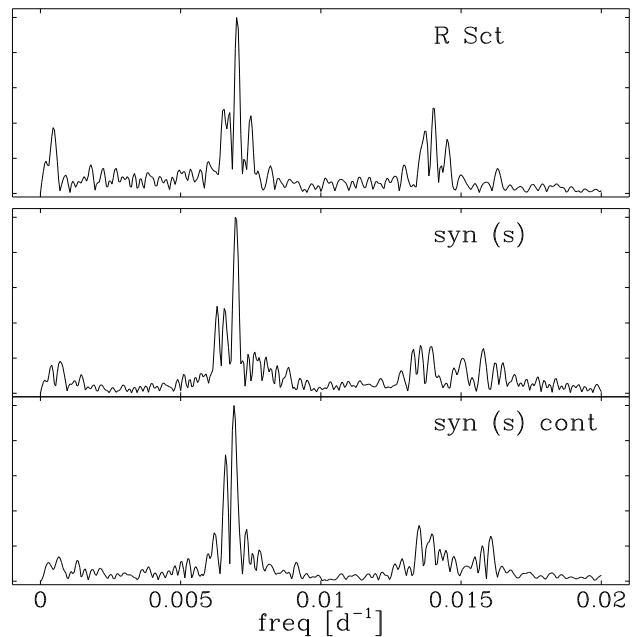


**Fig. 3.** Amplitude Fourier spectrum for the signals of Fig. 2.

The AAVSO observational data consist of visual estimates of the magnitude. A short typical sample of the raw observations (dots) is shown in Figure 1. One sees that the sampling can vary from excellent to poor. A statistical analysis of the data shows that the individual observations have a normal distribution with  $\sigma_s = 0.2$  that is indepen-

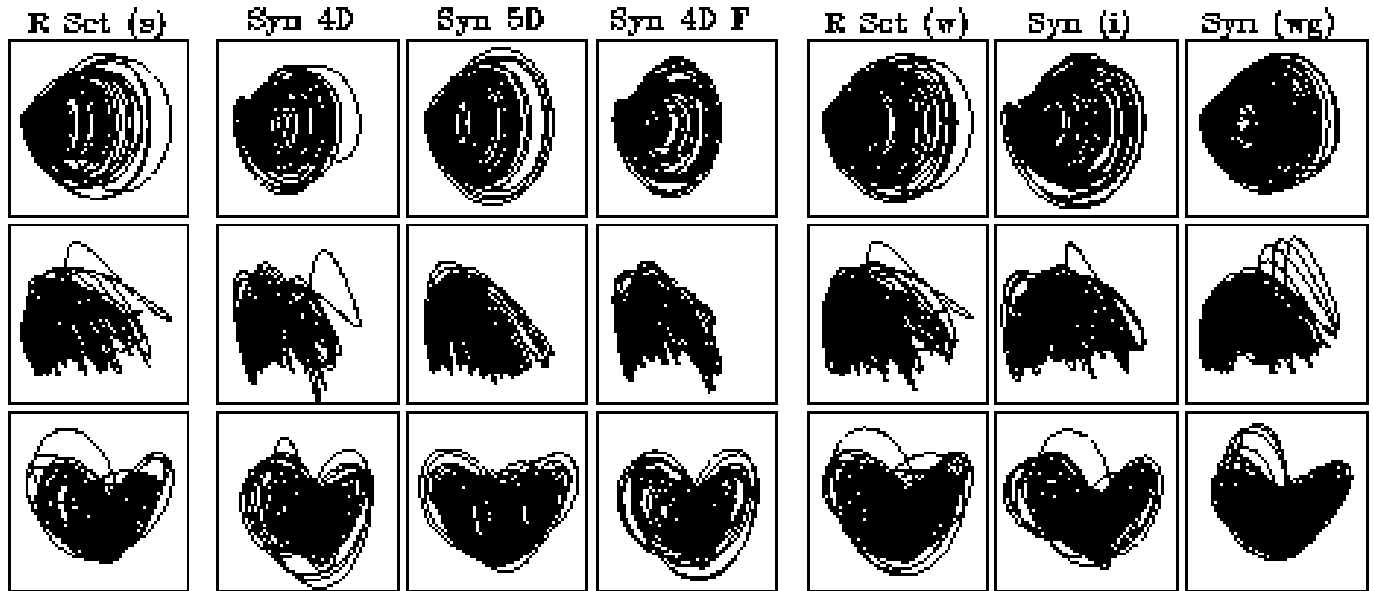


**Fig. 4.** Lowest 3 BK projections. *Col. 1:*  $s$  data set, 2–3: synthetic signals from map (*cf.* text), 4: synthetic *flow*, 5:  $w$  data set, 6 & 7: synthetic signals from  $i$  and  $w$  data sets. – NOTE: the quality of this figure is crappy due to xxx.lanl.gov requirements

dent of magnitude, presumably because of the logarithmic response of the human eye. We have thus chosen to work with the magnitude rather than with the luminosity.

Our preprocessing of the raw observations proceeds as follows. First, we average the data on 2.5 day intervals. The precise value of the averaging interval is not critical, as tests with 5 day averages have shown. These averaged data are then smoothed and interpolated with a cubic spline (Reinsch 1967) in which the only free parameter is the estimated noise level of the input data ( $\sigma_s$ ). The final standard deviation of the magnitude averages from the smoothed curve is thus determined by this quantity. The last step in the preprocessing of the data is a low-pass Fourier filtering with a frequency cut-off of 0.02 c/d at 3dB. We have also experimented with other smoothing techniques, such as Savitzky-Golay filtering (*e.g.* Press *et al.* 1992) and Fourier down-sampling (Sauer in WG94), which however, if anything, have been less satisfactory.

The final result of the preparation process is a data set  $\{g(t_n)\}$  that is sampled at constant 1 day intervals. In Fig. 1 we have shown the type of smoothed curve that we fit to the raw observational data. The fit misses somewhat the deep light-curve minima because of the smoothing and filtering that suppresses the high Fourier components.

In Figure 2, on top, we display the 5000 day, middle subset of the smoothed AAVSO data, which we label  $s$ . In most of our analyses, §4.1 - §4.3, we have used this  $s$  set, first because for reasons of an economy of time, and second because it appears more typical in the sense that it contains intervals of both small and large amplitudes. The whole ( $w$ ) 30 year AAVSO data set, to be analyzed in §4.4 set is shown in Figure 8 in which for reference the horizontal bar indicates the short ( $s$ ) subset.

The amplitude Fourier spectrum of the  $s$  data set is exhibited on top of Figure 3. (We do not show the Fourier spectrum for the  $w$  data set because it is very similar, *cf.* also Kolláth 1990 who has Fourier analyzed all available 150 years observations).

In the nonlinear analysis of §4 we shall find it convenient to use Broomhead–King (1987) (BK) projections which project onto the eigenvectors of the correlation matrix. These projections are optimal because on the one hand they are orthogonal and on the other hand they provide an optimal spread away from the diagonal. In the first column of Figure 4 we display plots of the lowest three BK coordinates  $\{x_k\}$  for the  $s$  data set. The successive rows show the ( $x_2$  vs.  $x_1$ ), ( $x_3$  vs.  $x_1$ ) and ( $x_3$  vs.  $x_2$ ) projections. In these and in the following BK plots the scaling of the axes is  $x_1:x_2:x_3 = 8:4:1$ . One notes that the  $w$  data set, displayed in column 5 looks very similar in BK projections.

Before we show our nonlinear analysis we will first apply two standard astronomical techniques to the observational data. Both are based on the assumption that the signal is multi-periodic, and we show that neither of them gives acceptable results.

### 3. THE FAILURE OF STANDARD LINEAR ANALYSES

#### 3.1. Fourier Decomposition

The first question one may want to address is whether a multi-period Fourier sum can give a good description of the data. We have therefore constructed a least-squares fit for a multi-periodic signal using, quite generously, the 35 most significant frequencies and their amplitudes and

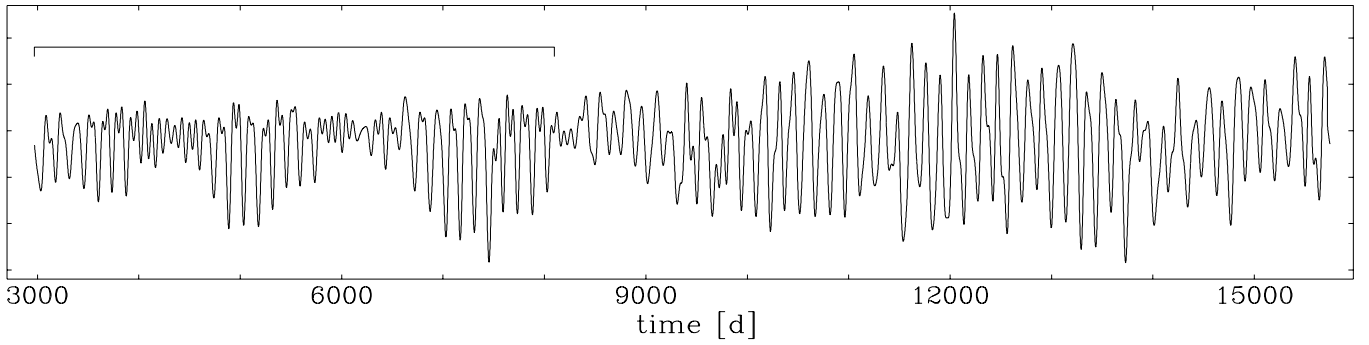


**Fig. 5.** Multi-periodic synthetic signal fitted to the  $s$  data set.

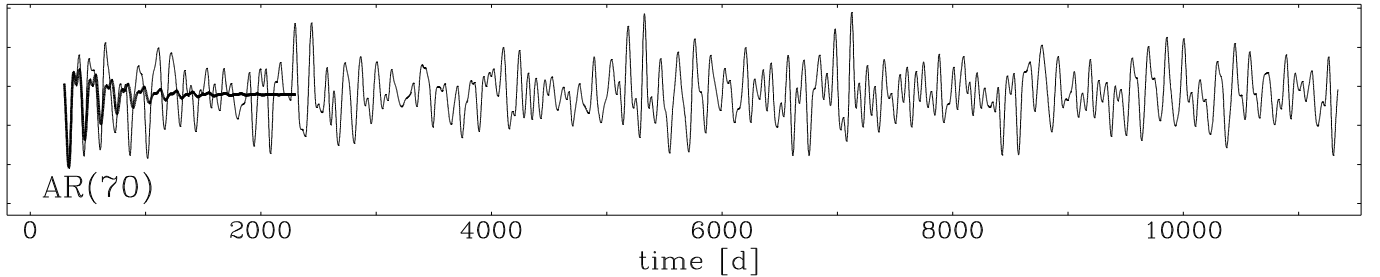


**Fig. 6.** A typical implementation of an autoregressive scheme.

phases (of the  $s$  set). (We have chosen a 70 parameter fit for future comparison purposes, because that will also be the number of parameters of the successful nonlinear map to be described in §4). For consistency with the following nonlinear analysis we have also used the smoothed signal for this analysis although the smoothing has little effect on the Fourier fit and on the conclusions we reach about its usefulness.

The multi-periodic Fourier fit is shown in Figure 5. A comparison with Fig. 2 shows that *it is quite good over the data set which is delineated with an overbar*. However, beyond the range of the  $s$  set it displays a behavior that ostensibly is *not compatible* with the observed R Sct data. This is even more convincing when the light-curve data over the last 150 years (Kolláth 1990) are considered. The Fourier expansion can thus serve as a good interpolation, but it fails miserably as an extrapolation. This should not really come as a surprise because it takes many coefficients and very strict phase-relationships to produce a signal with the kind of asymmetry that the observed light-curve possesses. In the extrapolated regime the phases act as if they were random and thus produce the much more symmetric signal seen beyond  $t=10\,000$  in Fig. 5 in which the characteristic RV Tau type alternations of deep and shallow minima disappear. In contrast, as we shall see, the nonlinear map not only fits the data set, but it also has predictive power in the sense that the nature of the syn-

thetic signals is very similar to the data set, independently of the epoch.

We also would like to point out that there is also a theoretical reason that militates against a multi-periodic interpretation of the light curve. The Fourier spectrum shows a large number of frequency peaks above the noise level that would have to be interpreted as modal frequencies or linear combinations thereof. There are however very few radial modes in the observed Fourier spectral range. Furthermore, the visual whole disk observations can detect nonradial modes up to  $\ell=3$  at best, and only the lowest few of these can be expected to be vibrationally unstable. There is thus a shortage of modes to explain the spectrum as multi-periodic.

The question arises whether the Fourier spectrum changes over the 150 years could be due to evolutionary changes in the structure of the star. The work of Kolláth (1990) has shown that the envelopes of the Fourier spectra are relatively steady for different sections of the available 150 years of data, but the individual peak structure is not. Even if, contrary to our previous conclusion, one could interpret the peaks as due to a very large number of excited modes, the observed frequency peaks in successive temporal segments do not appear to move in a systematic fashion with time as one would expect from an evolving star (which in addition would have to evolve much more rapidly than evolution theory indicates). A multi-periodic interpretation of the observed Fourier spectrum is there-

fore essentially incompatible with pulsation and evolution theories.

### 3.2. Autoregressive Analysis

We have also performed another common linear analysis, namely an AR fit which assumes that the signal is produced by a linear auto-regressive process with white noise (*e.g.* Scargle 1981, WG94). The physical picture behind this approach is that of a set of linear modes which are stochastically driven.

The thin line in Figure 6 represents an implementation of a 70 coefficient AR process, with a noise intensity such as to reproduce the overall amplitude of the observed fluctuations. The signal of Fig. 6 is plotted on the same vertical scale as the data set (Fig. 2). *The AR signal ostensibly again bears little resemblance to the s data set.* In contrast to the Fourier fit of the previous section, the AR extrapolation preserves some of the RV Tau-like alternations of deep and shallow minima, but it lacks the asymmetry of the observed light-curve. Using as many as 500 coefficients does not help. We note in passing that using an ARMA instead of this AR does not improve the signal either. The thick curve in Figure 6 shows the extrapolation of the AR process without noise, started on the data set.

We note that this AR analysis also dodges the question as to the mechanism which could provide a stochastic driving of sufficient strength to produce the observed irregularity.

The AR analysis again confirms that the dynamics that generates the signal is strongly nonlinear.

## 4. THE GLOBAL FLOW RECONSTRUCTION

Our nonlinear analysis falls under the general category of *global flow reconstructions* (*e.g.* ABST93) and the details of our approach are clearly documented in SKB to which we need to refer the reader. Space permits us to present only the gist of it here.

We assume that the pulsations are generated by a flow of the form of  $d\mathbf{Y}/dt = \mathbf{G}(\mathbf{Y})$ , where  $\mathbf{Y}(t)$  traces out the trajectory of the system in its  $d$ -dimensional *effective phase-space*. *A priori* we have no clue about the function  $G$ , nor even its dimension  $d$ . According to the embedding theorem there then exists a variable  $\mathbf{X}$  in the  $d_e$ -dimensional *reconstruction-space* which satisfies a nonlinear equation (map) of the form

$$\mathbf{X}^{n+1} = \mathbf{F}[\mathbf{X}^n], \quad (1)$$

The set of  $d_e$ -dim vectors  $\mathbf{X}^n = \{g(t_n), g(t_n - \Delta), g(t_n - 2\Delta), \dots, g(t_n - (d_e - 1)\Delta)\}$  can be constructed *from the*

*observed scalar variable*  $\{g(t_n)\}$ , in our case the star's magnitude, and the  $\{t_n\}$  are equally spaced times. The time-delay  $\Delta$  is an integer multiple of the spacing. The  $g$  variable is assumed to be a smooth function of the effective phase-space variable  $\mathbf{Y}$ , *viz.*  $\{g(t_n)\} \equiv \{g(\mathbf{Y}(t_n))\}$ . We will refer to  $\mathbf{X}^n$  as a *trajectory* because it maps out the temporal behavior of the system in the  $d_e$ -dim Euclidian reconstruction-space. (In §4.3 we shall also reconstruct a  $d_e$  dimensional flow (eq. 2) instead of the map of eq. 1.)

The physical trajectory  $\mathbf{Y}(t)$  is of course devoid of singularities and intersections, but the transformation (diffeomorphism) from  $\mathbf{Y} \in \mathbf{R}^d$  to  $\mathbf{X} \in \mathbf{R}^{d_e}$  can in general cause such ambiguities to appear in the trajectory  $\mathbf{X}^n$ . However when the dimension  $d_e$  is large enough all cusps and intersections become resolved and the transformation is then called an *embedding*, and the reconstruction-space becomes an *embedding-space*.

The embedding theorem establishes a one-to-one correspondence between the attractor points in the effective phase-space and the one reconstructed from the embedding variable. This is a very powerful result because some quantities are preserved in the embedding. It thus allows one to *infer quantifiable properties of an unknown underlying dynamics from the observations of a single quantity*, namely the magnitude in our case.

In SKB we have shown how the reconstruction analysis yields both a lower and an upper bound on the *a priori* unknown dimension  $d$  of the dynamics. In the case of R Sct it will turn out that the lower and upper limits coincide which will allow us to infer a definite dimension  $d$  for the dynamics.

The best choice for the global map  $\mathbf{F}$  is of course unknown. It is natural to try a polynomial expansion. Thus we assume  $\mathbf{F}(\mathbf{X}) = \sum_k \mathbf{C}_k P_k(\mathbf{X})$ , where the  $P_k(\mathbf{X})$  represent polynomials of order up to  $p$  that are *orthogonal on the data set*. In SKB we discuss how the polynomials are constructed and the coefficients are determined efficiently with a singular value decomposition (SVD) method.

Once we have constructed a map  $\mathbf{F}$  we can generate *synthetic* trajectories or signals *ad libitum* by iterating the map (eq. 1) with some seed value. The nontrivial question then arises how to compare the chaotic synthetic signals with each other and with the data set. Standard statistical comparison tests are not possible because of the small size of the data set. We are therefore obliged to resort to more subjective tests. The comparison of the appearance of the synthetic signal to the original one is usually not enough. For example, as we have seen in §3, multi-periodic signals can mimic the observational light variations, but the difference is quite obvious from the Fourier transform. Also, Fourier spectra have difficulty distinguishing between signals with amplitudes modulations of different lengths and depths. Our experience is (SKB) that in addition to the signal itself and its Fourier spectrum it is necessary also to compare projections of the reconstructed phase-space trajectories.

In SKB it has already been discussed how and why small changes in the smoothing, the polynomial order  $p$ , and the delay  $\Delta$  can change the synthetic trajectory between chaotic, periodic, or unstable. In the case of real data such as we consider here, there are additional parameters related to the filtering, the treatment of gaps, and the interpolation. *Prima facie*, this sensitivity may appear very disturbing, but is to be expected. Indeed, one recalls that even for the 1-D logistic map periodic cycles are intimately close to chaotic solutions as the parameter of the map is varied (O93). It is therefore no surprise that one witnesses here a strong sensitivity to the precise values of the coefficients of the polynomial map.

It is thus imperative to distinguish between *the robustness of the dynamics itself*, in particular the robustness of the structure and dimensionality of system (1), and *the extreme sensitivity of the integral curves or trajectories of this dynamics to the parameters of the maps*. The important point is to ascertain that *within a reasonably broad range of the above mentioned parameters chaotic solutions exist* and that their properties are robust. By robust we mean that the synthetic signals satisfy our three comparison criteria with the data set. Furthermore, we require that quantitative properties, such as the Lyapunov exponents and the fractal dimensions (*e.g.* O93) that we compute from the various synthetic data display a certain invariance over the range of good maps (see also SKB).

It sometimes happens that a map is unstable in the sense that an iteration of the map for the generation of a synthetic signal blows up. This can occur when the density of data points in regions of high divergence is insufficient to provide a stable neighborhood, and small changes in the nonlinear coefficients allow the orbit to be kicked away from the attractor.

Our methodology is to search for the best region of robust maps and synthetic signals by exploring the parameter-space of the three main quantities: the smoothing parameter, the time-delay and of course the embedding dimension. The order of polynomial expansion  $p$  plays a lesser role as long as it is large enough, but of course it is useful to find the smallest value. The number of SVD eigenvalues and their cut-off value (*q.v.* SKB), as well as the locations and widths of the gaps also come into play, but generally are less critical. A systematic search of the whole parameter-space is rather time-consuming so we have used the strategy of searching with one parameter at a time. After several 'iteration steps' we can generally find the best regime in parameter-space. If this regime is broad enough we claim success.

#### 4.1. Reconstructions with the $s$ data set

The typical behavior of the error between the observed values and the values predicted with the map as a function of the polynomial order  $p$  has already been shown in figure 1 of BSKM. There is a definite convergence as

$p$  is increased. More importantly the figure shows a clear levelling off beyond a value of  $d_e=4$ . While *this suggests a minimum embedding dimension of 4*, by itself however it is not sufficient and we have to ascertain that the 4D synthetic signals have the same properties as the data set and that the maps are robust.

We note though immediately that, consistently with the behavior of the error norm *we have not been able to find a single good 3D map* with synthetic trajectories that bear any resemblance to the R Sct data set. On the other hand, our extensive tests with the R Scuti show that the global flow reconstruction provides excellent maps in 4D with the parameters  $4 \leq \Delta \leq 7$ ,  $p = 4$ , and  $\sigma_s = 0.1$ . It thus appears that the minimum embedding dimension is indeed equal to 4 or greater. This conclusion will be further supported below by the fact that the fractal dimension of the attractor is also greater than 3.

Two contiguous sections of one of our best representative 4D synthetic signals ( $p = 4$ ,  $\Delta = 6$ ,  $\sigma_s = 0.1$ ) are displayed in Figure 2 (rows 2-3). The amplitude Fourier spectra of these two segments are also depicted in Figure 3.

The lowest 3 BK projections of the observations and several different sets of synthetic data are displayed in Figure 4. Although the maps have been obtained for various  $\Delta$  and  $d_e$ , when we want to make comparisons we have to construct the various BK plots with common parameters which throughout we have chosen as  $\Delta=2$  and  $d_e=8$ . The 4D synthetic signal shown in col. 2 has been constructed with  $p=4$ ,  $\Delta=5$ , and the 5D signal in col. 3 with  $p=3$ ,  $\Delta=7$ . For both the smoothing parameter is  $\sigma_s=0.10$ .

The synthetic signals themselves (Fig. 2), their Fourier spectrum (Fig. 3) and their BK projections (Fig. 4) are very similar, and *they are independent of the embedding dimension*. This strongly corroborates that *the minimum embedding dimension is indeed equal to 4*.

Our analysis has a number of free parameters and we now address the important question of the robustness of the results with respect to these parameters. It is the time-delay  $\Delta$  and the smoothing parameter  $\sigma_s$  that play the most important role in the analysis (SKB). A brief comparison of the effects of these parameters is therefore presented in Figure 7 for the lowest BK coordinate projection. The middle row corresponds to a value of the smoothing parameter  $\sigma_s=0.10$  for which we obtain the best maps. In SKB we have found that a value of  $\sigma_s$  is equal to the actual noise level gives the best maps. Here we do not know the exact value of the average observational error, but the error for the averaged magnitudes is in the range  $\sigma_s=0.04-0.20$  depending on the number of observations in the 2.5 day bins. The optimal smoothing level is thus in agreement with the level of the observational noise. We note that good maps are obtained for a range of  $\Delta$  values from 4 to 10 (except for a limit cycle at  $\Delta=9$ ).

*A priori* we had not idea what values to choose for  $\Delta$ , or even whether any values could be found for which one

obtains a good map that captures the dynamics. All we could expect is that for small values the map would be close to linear, but since the trajectory is then collapsed to the diagonal noise would overwhelm the reconstruction. On the other hand for large  $\Delta$  the map could become so nonlinear that perhaps a polynomial representation would be inadequate. Our results show that indeed there exists a region of  $\Delta$  in which good maps can be obtained.

Fig. 4 also demonstrates that with over-smoothed data ( $\sigma_s=0.12$ ) the maps do not give complex enough synthetic curves. The plots clearly indicate some multi-periodic (n-torus) behavior with distorted Lissajous-like curves for lower time-delays. In contrast, the slightly under-smoothed light-curve ( $\sigma_s=0.09$ ) shows that chaotic signals are possible, but that the maps are more unstable (we cannot iterate for more than some 20–30 thousands of iterations, at most).

The low pass filtering following the spline smoothing helps in the construction of good robust maps, presumably because a reduction of the high frequency power decreases the nonlinearity of the signal. We have to note that with larger  $\sigma_s$  in the spline smoothing we can obtain relatively good results without the Fourier filtering. However, we obtain the best results with combined spline smoothing and Fourier filtering. While a purist might object to this distortion of the signal and hence of the attractor, we think that we merely remove sharp features which do *not* affect the essence of the attractor nor the physical interpretation that we will give of the dynamics.

We have also tested the sensitivity to sampling rate. The results remain relatively good with a time-step of 2 days, but an even lower sampling rate destroys the similarity between the light-curve and the synthetic signals. We attribute this breakdown to the polynomial map which may not be able to handle the increased nonlinearity.

There is one more parameter controlling the reconstruction of the map with the SVD procedure (Press *et al.* 1992), namely the eigenvalue cut-off  $\omega_c$ . The number of combinations of monomials goes up very quickly with  $p$  and  $d_e$  as  $C_{d_e+p}^p$  (*e.g.* Casdagli 1992) and their independence over the data set decreases rapidly, as indicated by small SVD eigenvalues. The purpose and power of the SVD method are that by using such a cut-off, typically at machine precision ( $10^{-14}$ ), one automatically selects the most important combinations of monomials, and one rejects the others which give numerical problems in Gram-Schmidt polynomial constructions or in QR decompositions. The cut-off  $\omega_c$  is here defined as the ratio of smallest to largest SVD eigenvalue. For most calculations, as long as we keep  $p$  small, we can use all the meaningful eigenvalues for the reconstruction (For example in 4D with  $p = 4$  there are 70 eigenvalues, all of which are above the cut-off). Actually, the synthetic signals generally are insensitive to  $\omega_c$  as long as  $\omega_c < 10^{-10}$ , and as long as  $\omega_c$  does not exceed ten times the ratio of the smallest to the largest eigenvalue. For larger values of  $\omega_c$  the map loses

**Table 1.** Reconstructed Lyapunov exponents [ $d^{-1}$ ] and Lyapunov dimension

$d_e$	$\Delta$	$p$	$\lambda_1$	$\lambda_3$	$\lambda_4$	$d_L$	note
4	4	4	0.0019	-0.0016	-0.0061	3.05	[0]
4	5	4	0.0017	-0.0014	-0.0054	3.06	[0]
4	6	4	0.0019	-0.0009	-0.0051	3.19	[0]
4	7	4	0.0020	-0.0011	-0.0052	3.18	[0]
4	8	4	0.0014	-0.0010	-0.0049	3.07	[0]
5	7	3	0.0016	-0.0005	-0.0041	3.27	[0]
6	8	3	0.0022	-0.0003	-0.0018	3.52	[0]
4	6	5	0.0013	-0.0004	-0.0036	3.26	[1]
4	6	5	0.0015	-0.0011	-0.0030	3.15	[2]
4	6	5	0.0015	-0.0013	-0.0039	3.04	[3]
[0] <i>s</i> set, [1] <i>wg</i> set, [2] <i>w</i> set, [3] <i>i</i> set							

flexibility ('under-fits') and we usually obtain limit cycles and fixed points.

In BSKM we had inserted a small gap where we had estimated that the data were not good enough to give a reliable interpolation. Further tests have shown that the reconstruction is not very much affected by the presence of absence of these gaps.

The Gram-Schmidt construction that has been used in BSKM to generate the polynomials and the map is much less robust and is more prone to round-off errors than the SVD approach we have used subsequently in SKB and here. Furthermore, our search for regions of good maps was somewhat less thorough in BSKM. The synthetic signals here are therefore slightly different from BSKM although our conclusions are immune to this kind of detail.

#### 4.2. Lyapunov exponents and fractal dimension

The important quantitative characteristics of chaotic systems (such as Lyapunov exponents and fractal dimension, *e.g.* O93) cannot be obtained directly from the short observational data, but such calculations are possible for synthetic signals because these can be computed for several hundred thousand points. In order to give an indication of the robustness of the Lyapunov exponents and the Lyapunov dimension we show in Table 1 their variation with embedding delay. The errors are about  $10^{-4}$  on the exponents, and about 0.02 on  $d_L$ . The positive Lyapunov exponent is seen to be quite robust. The negative ones show more scatter, but that is to be expected (ABST93).

For all the chaotic synthetic trajectories the second Lyapunov exponent is *always* smaller than  $10^{-4}$  ( $\lambda_2$  has therefore been omitted from Table 1. This fact turns out to be very important. Indeed, had we constructed a flow rather than a map one of the exponents would have been exactly zero. Such a flow, on the other hand, when sampled at discrete time-intervals becomes equivalent to a map. When the sampling time is sufficiently short, as it



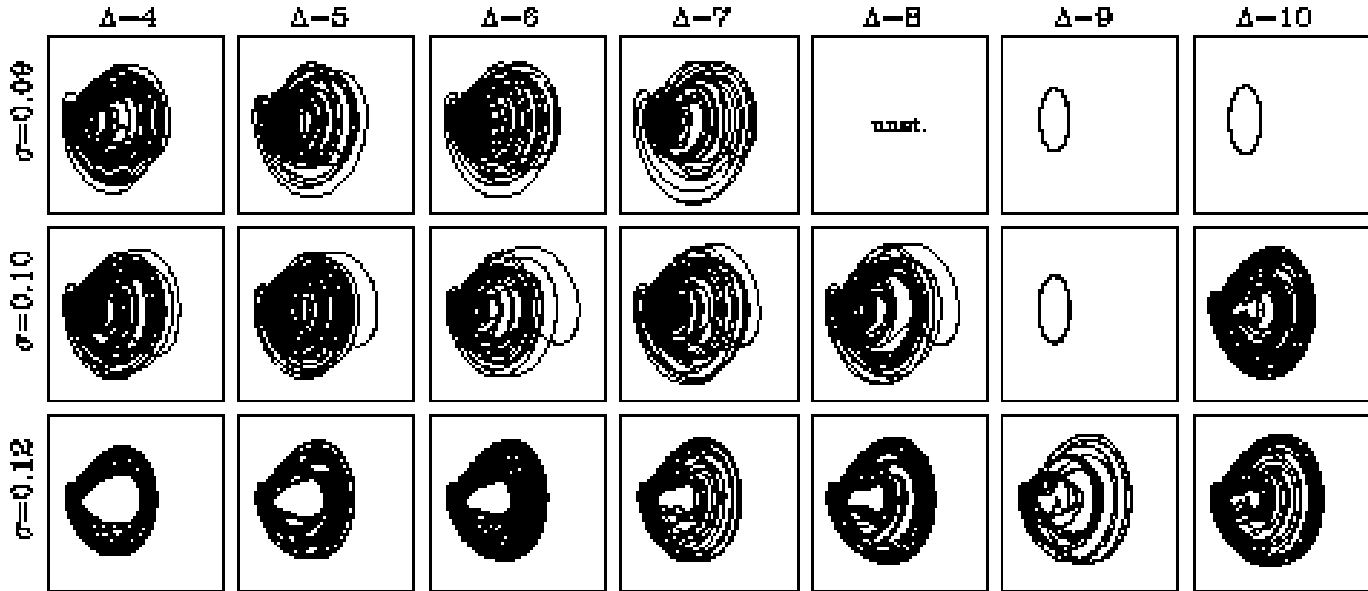


Fig. 7. Lowest BK projections (4D maps) for different values of  $\Delta$  and  $\sigma_s$ . – NOTE: the quality of this figure is crappy due to xxx.lanl.gov requirements

is for R Sct, the Lyapunov exponents of the map and the flow should be very close to each other. *The smallness of  $\lambda_2$  thus provides a very strong independent check on our analysis and on the basic assumption that there is a low-dimensional flow that determines the behavior of the star.*

We find that there is perhaps a tendency for the Lyapunov dimension to increase (and to deteriorate, if we make a parallel with SKB) as we increase  $\Delta$ , presumably caused by the need for an increase in the map’s nonlinearity. There is a similar behavior with embedding dimension. This deterioration is almost certainly related to the decrease in the density of points in higher dimensional embedding-spaces.

The positive sign of at least one Lyapunov-exponent (*i.e.*  $\lambda_1 > 0$ ) guarantees that the attractor is chaotic. The inequality,  $\lambda_1 + \lambda_2 + \lambda_3 > 0$ , which is very solidly satisfied, implies that the *fractal Lyapunov dimension  $d_L$  is greater than 3* (O93). In no case have we ever found 2 positive Lyapunov exponents (hyper-chaos).

Table 1 also reveals the important fact that *the Lyapunov exponents and dimension are essentially independent of the embedding dimension  $d_e$* , as long as  $d_e \geq 4$ . (The slight increase of  $d_L$  with  $d_e$  is most likely due to the deterioration of the method because of a decrease in point density with embedding dimension). If a high-dimensional dynamics were at the origin of the R Sct pulsations  $d_L$  would have increased essentially as fast as  $d_e$ .

We have further calculated the correlation dimension  $d_2$  (O93). Because an accurate computation of  $d_2$  necessitates extremely large data sets and because the correlation dimension can be contaminated by systematic deviations, we estimate our error on  $d_2$  to be about an order of magni-

tude greater than for  $d_L$ . The correlation dimension is also known to underestimate sometimes the fractal dimension (see *e.g.* Gouesbet 1991). This could be the reason that our estimates give  $d_2 = 2.8\text{--}2.9$ , *i.e.* values smaller than 3. These values are however compatible with the theoretical ordering  $d_2 \leq d_1 \leq d_0$  (O93), assuming the Kaplan-Yorke conjecture, *i.e.*  $d_L = d_1$  to hold.

The embedding theorem involves the box-counting dimension  $d_0$ . We have not computed  $d_0$ , but from the difference between  $d_L$  and  $d_2$  we have reasons to believe that all three dimensions are close to each other. In fact, according to the embedding theorem, to make a difference,  $d_0$  would have to be greater than 3.5. From the fractal dimensions one therefore infers an upper limit  $d_e \leq 7$ . This seems to be a very generous upper limit, because our analysis has shown that we can get excellent embeddings already in  $d_e=4$ . We caution though that we cannot be entirely sure that we have avoided all trajectory singularities in 4D.

### 4.3. Flows

Up to this point we have searched for embeddings with *maps*. It may therefore be objected that while we have been able to construct nonlinear maps from the data set, this does not guarantee that there exists a corresponding *flow* in the effective phase-space (although the systematic smallness of the second Lyapunov exponent has already given a strong hint that a flow exists).

It is therefore important to test whether an embedding flow can be constructed directly from the data (SKB), *i.e.* whether we can find a nonlinear function  $\mathbf{H}$  such that

$$d\mathbf{Z}/dt = \mathbf{H}(\mathbf{Z}), \quad (2)$$

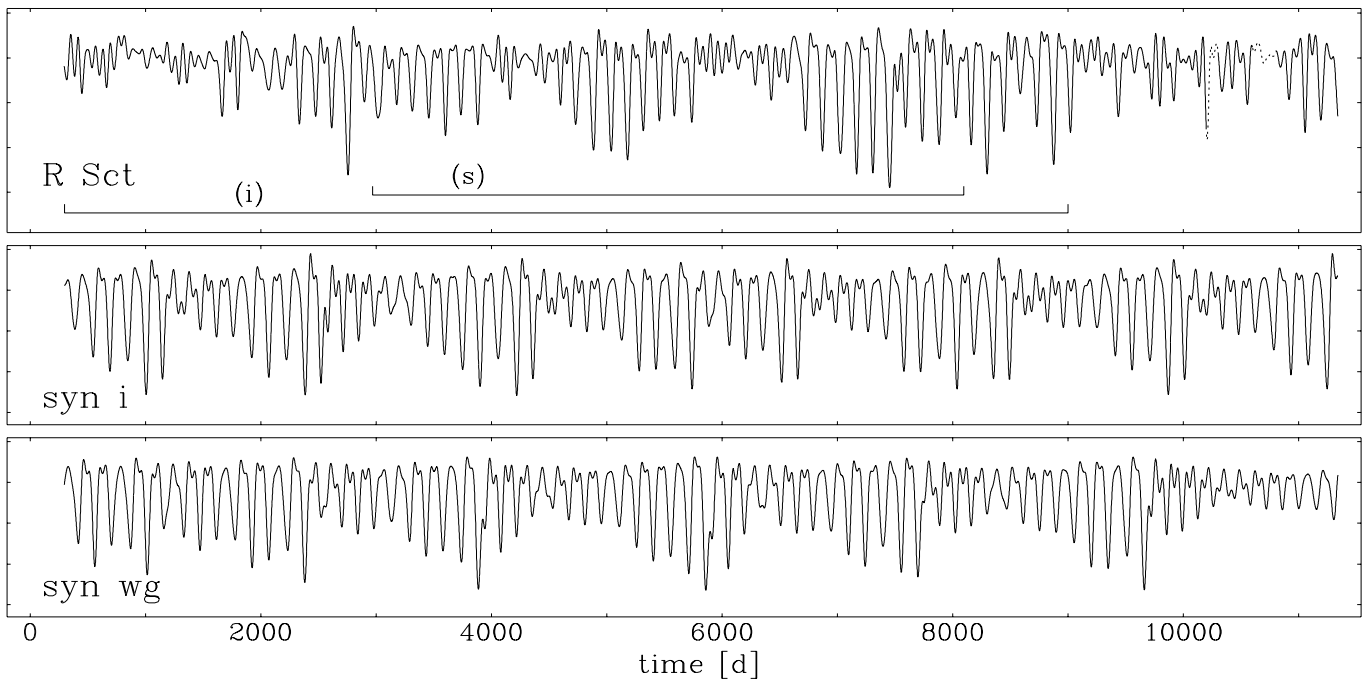


**Fig. 8.** *Top:* The whole ( $w$ ) smoothed AAVSO light curve of R Scuti, Julian Day 2,438,000+. *Below:* synthetic signals from  $i$  and  $wg$  data sets, respectively.

where  $\mathbf{Z}(t)$  is such that  $\mathbf{Z}(t_n) = \mathbf{X}^n$ . Since we only know the function  $\mathbf{Z}$  on a discrete set of points we approximate the derivative by a discrete Adams–Moulton scheme (as suggested by Brown, Rulkov and Tracy 1994).

We find that embedding flows exist for almost all the parameters for which maps exist, and that their synthetic trajectories have a very similar behavior. (We generate the synthetic signals by integrating the system by a fourth order Runge-Kutta scheme with a fine time-step  $\delta t = 0.001$ ). However, the flows tend to be somewhat less stable than the maps, *i.e.* the integration typically blows up after some ten thousands days. Column 4 of Fig. 4 shows the BK projections for the best flow.

#### 4.4. Other tests

Suppose we create a noisy, multi-periodic signal with a Fourier power-spectrum that is very similar to the observational signal, but with different phase-relationships. Can we fool the global reconstruction. method into believing that we have presented it with a low dimensional nonlinear flow? We have thus produced an artificial signal with the most important 35 frequencies and amplitudes of the observational data, but have then randomized the phases. Low dimensional polynomial maps constructed from this artificial data set are incapable of producing synthetic signals with similar appearance! From a nonlinear dynamics point of view of course this is not surprising because the artificial signal is multi-periodic and thus needs an embedding-space of a dimension at least equal to  $2 \times 35$ .

The question also arises whether one might, erroneously, extract a low-dimensional chaotic dynamics from a fully stochastic data set. In theory this is not possible, but it cannot be ruled out that for a real, noisy data set one might find parameter combinations for which the maps give low-dimensional chaotic synthetic signals. However we deem it somewhat unlikely that there would exist a *range* of parameters in which a robust map could be found. As a test we have constructed a further artificial stochastic signal by filtering Gaussian white noise with the envelope of the Fourier transform of the R Scuti data. Again we could not make a good reconstruction of these data. The synthetic signals were always limit cycles which represented some average of the trajectory (*cf.* also SKB).

#### 4.5. Reconstruction with longer data sets

In the preceding analyses we have only used a subsection ( $s$  data set) comprising the middle half of the AAVSO observations (*cf.* Fig. 2). This restriction to a subset of the whole data has been convenient because of running-time economy for the large number of tests that we have made. The choice of this particular stretch of data has been dictated by its typical nature with both large and small amplitudes.

We now turn to an analysis of the whole AAVSO data set which is shown on top of Fig. 8. We consider two slightly different versions of smoothed data sets, one without gaps ( $w$  set) and one ( $wg$  set) with two gaps located

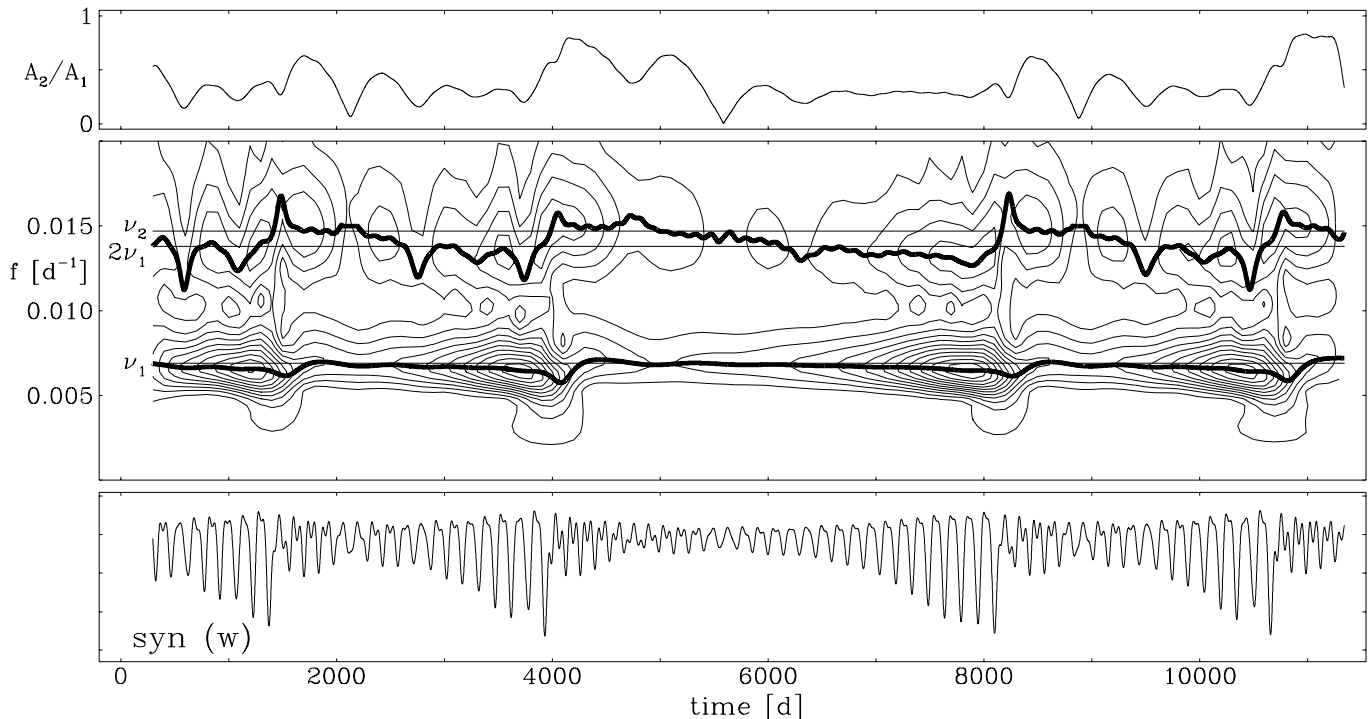


**Fig. 9.** Wavelet analysis. *Top:* Amplitude ratio, *middle:* Amplitude contours, *bottom:*  $w$  synthetic signal from  $w$  set.

at  $(10\,200 < t < 10\,300)$  and  $(10\,600 < t < 10\,800)$  where the observational data are very sparse and the light-curve is poorly defined (the dotted part of the curve represents the interpolation through the gaps). For reference, the horizontal bars in Fig. 8 denote the lengths of the  $s$  and  $i$  data sets.

The BK projections of the  $w$  set are displayed in col. 5 of Fig. 4. They are seen to be hardly distinguishable from those of the  $s$  data set, even though the light-curve itself appears somewhat different qualitatively. The envelopes of the Fourier spectra of the  $s$  and  $w$  data sets are essentially the same as well.

In Fig. 8 we exhibit the best 4D synthetic signal 'syn  $wg$ ', obtained with  $p = 4$ ,  $\Delta = 6$  and  $\sigma_s = 0.13$ . In column 7 of Fig. 4 we display its BK projections.

Even though these maps have been constructed with the  $wg$  data set the synthetic signals bear a stronger resemblance to the  $s$  data set, as Fig. 8 shows. In fact, the agreement with the  $wg$  data set itself is perhaps not as satisfactory as one would like. The low amplitude, relatively more erratic behavior in the last 1500 days is not well mimicked by the synthetic signals, although their Fourier spectra and the BK projections are quite similar to those of the  $wg$  set.

In view of the slight, but definite deterioration of the reconstructions with the longer data set we have therefore also considered a number of sets of intermediate lengths. In Fig. 8 we have delineated one such set ( $i$ ), which comprises all the data with  $t \leq 9000$ . The best 4D synthetic

signal that we obtain from this  $i$  set is displayed in row 2 of Fig. 8 ('syn  $i$ ') and its BK projections are shown in column 6 of Fig. 4. The best parameters are the same as for the  $wg$  set, *viz.*  $p = 4$ ,  $\Delta = 6$  and  $\sigma_s = 0.13$ . The synthetic signal bears a good resemblance to the  $i$  set, but the maps again seem somewhat reluctant to give long stretches of low amplitude behavior such as occur for  $t < 1500$  in the  $i$  data set. From Table 1 we see however that the Lyapunov exponents and Lyapunov dimensions are the same as for the synthetic signals generated from the  $s$  set.

Generally we find that extending the  $s$  data set to the left (earlier data) has little effect on the maps and on the shape of their synthetic signals. On the other hand, when we add later data (on the right), the maps become more sensitive to the parameters and to the location of the gaps. Furthermore, even the best maps do not reproduce quite as well as one would like the low amplitude behavior seen in the AAVSO data for  $t > 9000$  in row 3 of Fig. 8. Below we shall return to a discussion of the possible reasons for these discrepancies.

Another feature of the reconstructions from the longer data sets is the enhanced sensitivity of the synthetic signals to small changes in the parameters, and thus in the maps. For example, the synthetic signal (' $wg$ ') shown in Fig. 8 has been generated by a map that uses only 58 of the total of 70 SVD eigenvalues that occur with  $d_e = 4$  and  $p = 4$ . The use of all 70 eigenvalues causes a change of the order of 0.001% in the map over the observed data. (We compare here the average values of the daily predictions

of the two maps calculated on the data set). On the other hand, if we compute similarly the daily predictions on a synthetic data set, the differences in prediction between the two maps jump to 10–20%. This shows that the two maps are very similar on the attractor, but that they become quite different in its vicinity. The use of more than 58 eigenvalues results in more regular synthetic signals, some of which can even be limit cycles.

A similar sensitivity is observed with respect to the locations and lengths of the gaps that we introduce in the data sets. For the ungapped  $w$  set, for example, we obtain a chaotic signal with an amplitude modulation time-scale that, compared to 'syn  $wg$ ', is almost a factor of 2 longer (bottom, Figure 9). The pulsation amplitude grows much more slowly from small to large with a 'more regular' appearance; then, in a briefer irregular phase the signal collapses to small amplitude.

This behavior gives us a clue as to the origin of the sensitivity. Indeed it is very reminiscent of what can occur in the proximity of a Shilnikov-type *homoclinic connection* (e.g. Glendenning & Tresser 1985). It then suggests that we look for the fixed points of the maps and their linear stability roots. From the polynomial expressions of the maps they are easy to locate. In all the maps we find a fixed point located at the center of the attractor, and its two pairs of linear stability roots are always spiral. In Table 2 we display these two roots,  $\pm 2i\pi\nu + \rho$ , for the best synthetic signals for the  $s$ ,  $i$ ,  $wg$  and  $w$  data sets. First one notes that the two frequencies are almost invariant, and that they correspond closely to the dominant frequency peaks of the Fourier spectrum (Fig. 3).

**Table 2.** Linear stability roots of fixed point of the maps

data set	$\nu_1$	$\rho_1$	$\nu_2$	$\rho_2$
$s$	0.0068	0.0044	0.0145	-0.0062
$i$	0.0069	0.0009	0.0147	-0.0019
$wg$	0.0069	0.0004	0.0147	-0.0013
$w$	0.0069	0.0001	0.0147	-0.0012

There is a strong correlation between these roots and the behavior of the corresponding synthetic signals. Consider first the  $w$  signal (shown on the bottom of Fig. 9) and its roots. We interpret the signal as that of a trajectory that expands slowly ( $\nu_1/\rho_1 = 70$ ) along the mildly unstable spiral manifold with the corresponding *lower frequency*  $\nu_1$  of 0.0069 c/d dominating. Then this trajectory transits to the strongly attracting ( $\nu_1/|\rho_2| = 6$ ) spiral manifold. Here the higher frequency dominates the pulsation. This second phase is shorter consistently with the larger ratio  $\rho_2/\rho_1 = 12$ .

This interpretation is corroborated by a wavelet analysis of the  $w$  synthetic signal. For details of this analysis we refer to Kolláth & Szeidl (1993). In Fig. 9 (middle) depicts the amplitude contours in a frequency – time

space. The thick line represents the instantaneous frequencies  $f_{inst,k}(b=t) = \partial\phi(f_k, b)/\partial b$ , where we have chosen  $f_1 = 0.007$  and  $f_2 = 0.015$ , respectively, i.e. the dominant frequency peaks in the Fourier spectrum (the precise values of  $f_k$  are not critical because of the flat behavior of the phases in the vicinity of these frequencies). On top of Fig. 9 we record the ratio of the two wavelet amplitudes at  $f_{inst,k=1,2}$ . The shift back and forth between the harmonic  $2\nu_1$  and  $\nu_2$  is nicely brought to light by the wavelet analysis. For example, in the expanding stretch from  $t \approx 2500$  to 4000 the high frequency component of the wavelet is dominated by the harmonic  $2f_1 \approx 2\nu_1 = 0.138$ , but during the subsequent attracting phase, from  $t \approx 4000$  to 5700 the high frequency component shifts to the second frequency  $f_2 \approx \nu_2 = 0.0147$ . (The thin horizontal lines in Fig. 9 are drawn at these two frequencies.)

The behavior of the other synthetic signals and the values of their stability roots further corroborate this scenario. Thus, for example, for the  $s$  synthetic signal, the roots have a ratio  $\rho_2/\rho_1 \approx 1.4$ , and, in addition, compared to the frequencies, the growth rates are now by a factor of 5 larger. This is the reason for the more rapid amplitude variations of the  $s$  synthetic signal (Fig. 2) in which the expanding and contracting phases are therefore also closer in length. Furthermore, Table 2 shows that the real part of the first root ( $\rho_1$ ) is very sensitive. It is thus not astonishing that for some parameter values  $\rho_1$  becomes negative and the synthetic signal becomes a fixed point. For positive  $\rho_1$  the flow can also produce limit cycles instead of chaotic trajectories (e.g. Glendenning & Tresser 1985) as Fig. 7 indicates.

The evidence is seen to be strong that there exists a nearby homoclinic connection in the maps (and, by inference, in R Sct itself) which can explain the sensitivity of the long-term amplitude modulation to the parameters. In further support of this scenario we recall that the Lyapunov exponents and Lyapunov dimension of the synthetic trajectories are essentially invariant, suggesting that *the dynamics itself is quite robust despite the extreme sensitivity of the synthetic signals*.

We now return to possible reasons for the deterioration of the synthetic signals when, instead of the  $s$  subset, the whole AAVSO data set is used.

As already mentioned Fig. 8 indicates that compared to the  $s$  set there seems to be a qualitatively somewhat different behavior for  $t > 9000$ , with smaller amplitudes and a little more irregularity, and similarly perhaps for  $t < 2000$  as well. In particular, one notes that outside the  $s$  set there are very few deep minima. Extending the data set beyond the  $s$  set therefore provides no additional information about that part of phase-space.

We believe that it is the large relative noise level in the low amplitude behavior (the observational error is about constant  $\approx 0.1$ – $0.2$  mag throughout the data set) that affects our ability to construct maps that reproduce the long

low amplitude modulations. Evidence for the nefarious effects of large noise intensity has already been presented in SKB: (a) when large levels of noise were added to a chaotic signal the reconstruction often led to limit cycles which represented merely an average behavior of the pulsations, and (b) in an artificial signal that was composed of a limit cycle plus colored noise the reconstruction ignored again the stochastic component and recovered the average cycle. In our situation here, instead of a limit cycle, the 'average' behavior is chaotic. In addition this average chaotic behavior is dominated by the large amplitude pulsations that occur in range of the  $s$  set only. This can be the reason why the best synthetic signals systematically tend to have an appearance so similar to the  $s$  data set.

We need to mention an alternative, less likely, but also less comfortable explanation which might be found in the tacitly assumed constancy of the stellar parameters and of the map. Evolution time-scales for RV Tau stars have been estimated to be of the order of hundreds or thousands of years (Gingold 1974). Could it be that the tiny structural changes in the evolving star cause large changes in the nature of the trajectory in view of the strong sensitivity of the signal to small changes in the map parameters? We therefore caution that this constancy is an assumption. However it is a necessary working hypothesis as it would obviously be impossible to gain much useful information from such stars if the parameters were changing over a time-interval of the length necessary to sample the attractor.

Notwithstanding the difficulty of the reconstruction to reproduce synthetic signals with sufficiently long pulsational lulls it needs to be stressed again though that the Lyapunov exponents and Lyapunov dimensions are robust, suggesting that the reconstructed dynamics itself is robust, and close to the actual dynamics of R Sct.

#### 4.6. Spectral Analysis

In addition to the Fourier spectra that we have already presented, we have also computed a 70 parameter MEM spectrum. The MEM spectrum of the data has just two peaks and represents essentially an envelope of the Fourier spectrum although the peaks are somewhat broader.

We now address briefly the connection between the Fourier spectrum and the map. From our best 4D map we can construct a pseudo-MEM (amplitude) spectrum,

$$A(f) = \left| \frac{1}{1 - \sum_{k=1,4} a_k e^{-2i\pi((k-1)\Delta+1)f}} \right| \quad (3)$$

(eq. 7, WG94), where the  $a_k$  represent the *linear* coefficients of the 4D map around its fixed point. This 4 parameter pseudo-MEM spectrum again has two peaks with about the same widths as the envelope of the Fourier spectrum, and is actually better than the 70 parameter MEM

spectrum itself. The locations of the two peaks of the pseudo-MEM spectrum coincide almost exactly with the two frequencies of the linear stability analysis,  $\nu_1$  and  $\nu_2$  of Table 2. (It is interesting to point out that a comparable 4 parameter MEM spectrum misses considerably *both* peaks). The pseudo-MEM low frequency peak at 0.0069 c/d is also very close to its counterpart in the Fourier spectrum of R Sct, *i.e.* Fig. 3. The high frequency peak, on the other hand, occurs at  $\approx 0.0147$  c/d, which is somewhat higher than it is in the Fourier spectrum. This may not be a real discrepancy, and is likely to be related to the unsteadiness of the signal. Indeed, a comparison of the Fourier spectra of two sections of the same synthetic signal in Fig. 3, middle and bottom, shows a broad, unsteady structure at and beyond the first harmonic. This is caused by the continual switching back and forth between the harmonic of the first frequency ( $2 \times 0.0069$ ) and the second frequency 0.00147 c/d, as uncovered by the wavelet analysis.

The pseudo-MEM spectrum is well defined only when there exists a corresponding stationary AR process, which is not the case here. When we iterate the linear part of the map the amplitude of the lower frequency oscillation increases without limit, and at the same time the higher frequency oscillation evanesces (the rates of growing and decaying is given by the linear stability roots in Table 2). The nonlinear part of the map is needed to limit the amplitude and to transfer power to the higher frequency. This implies that the amplitude ratio of the peaks in the pseudo-MEM spectrum has no physical meaning.

## 5. DISCUSSION

We have presented evidence that the pulsations of R Scuti are *not* multi-periodic and that they are *not* generated by a linear stochastic process either, a process which, in any case would be hard to justify on physical grounds. Rather our global reconstruction has shown that the dynamics of R Sct, while noisy, is nonlinear and low-dimensional instead. This result is relatively robust with respect to the most important free parameters of the method, such as delay-time and smoothing.

We can, however, go further and extract information which will be physically useful. To start, of great interest is the dimension  $d$  of the inertial manifold, *i.e.* the manifold in which the dynamics evolves. This dimension  $d$  is obtained as follows. From the fractal Lyapunov dimension  $d_L \approx 3.1$  and the condition that  $d_L < d$  (integer) we infer a *lower limit*  $4 \leq d$ . On the other hand, from our nonlinear analysis we have inferred an *upper bound*  $d \leq d_e = 4$ . We thus arrive at the important conclusion that the dimension of the inertial manifold is indeed equal to 4.

What do the 4 dimensions that we thus have found mean in simple terms? A 4D embedding implies, remarkably, that the behavior of the complicated, seemingly erratic light-curve on any given day is *uniquely* expressible

in terms of the behavior of the 4 preceding days only (taking  $\Delta=1$  in eq. 1 for the sake of argument). In the context of a flow this is the number of independent variables or ODEs which are sufficient to generate the observed signal.

The reader may then wonder why R Sct is so different from, say a beat RR Lyrae star which, if it has 2 modes excited, would also be 4-dimensional. The only real difference is in the coefficients of the maps of the two types of stars: the RR Lyrae map produces an 2-torus (multi-periodic pulsation), whereas the R Sct map yields a strange attractor (chaotic trajectory). The physical reason why large amplitude chaotic behavior is not possible in RR Lyrae is that these stars are only weakly nonadiabatic (the growth-rate to period ratio is of the order of a percent), implying that amplitude modulations occur on a much longer time-scale than the pulsation itself (mathematically, the dynamics evolves on a near *center manifold*, cf. below). On the other hand, RV Tau stars are very far from adiabatic, a fact that allows modulations on the time-scale of the period itself, obviously a necessary condition for chaos.

In the literature *first return maps* have been plotted for RV Tau stars in the hope that they might yield a clue as to the possible chaotic nature of these objects (Veldhuizen & Percy 1989; Saitou *et al.* 1989), but disappointingly the first return maps turn out to be more or less scatter diagrams. In Figure 4 of Buchler, Kolláth and Serre (1995) we juxtapose the first return map for our short R Sct data set with a first return map of the best synthetic signal, both constructed with the minima  $\{m_i\}$  of the light-curve (*i.e.* a plot of  $m_{i+1}$  vs.  $m_i$ ). The synthetic signal gives a more compact plot, but which nevertheless has a great deal of structure, much more than one obtains for example with the Rössler band (*e.g.* Thompson & Stewart 1986). This indicates that *1D return maps cannot capture* the dynamics of R Sct, and is a reflection of the differences in the Lyapunov exponents and fractal dimensions of the two systems.

## 6. PHYSICAL IMPLICATIONS

We have demonstrated that the simplest and most natural explanation of the pulsations of R Sct is that they are produced by a 4-dimensional intrinsic dynamics. This dimension of four implies that 4 coordinates (or variables) are sufficient, and necessary, to describe the dynamics. The question is then how this low dimension comes about, and what the physical nature of these four variables is.

The hydrodynamics equations that describe the behavior of the star involve a continuum (*e.g.*  $\rho(\vec{r}, t)$ ,  $\vec{u}(\vec{r}, t)$ ,  $s(\vec{r}, t)$ , ...). However, it is possible to project these equations onto the space of the normal modes (linear eigenvectors) of which there is a denumerable infinity (a similar, but much simpler example is afforded by a vibrating

string or drum). The *configuration space*, in the parlance of WG94, is thus infinite-dimensional for a pulsating star.

Our past theoretical work on Cepheids and RR Lyrae stars (*e.g.* Buchler 1993) has shown that a description in terms of a few radial modes gives excellent agreement with observations as well as with numerical hydrodynamical simulations. These particular stars are weakly 'nonadiabatic' (dissipative), *i.e.* the ratios of growth-rates to oscillation-frequencies are small for the excited modes, at most of the order of a few percent, implying that the dynamics evolves on a center manifold (erroneously called 'slow manifold' in Buchler 1993). Our understanding of this *dimensional reduction*, from infinite to a dimension of a few, is solidly based on center manifold theory (*e.g.* Guckenheimer & Holmes 1983).

In contrast, W Vir and RV Tau stars are much more dissipative (large relative growth-rates, of the order of tens of percent), and there is no longer a center manifold. However, both experiments and theory have shown that the dynamics of dissipative fluids also often occur on low-dimensional manifolds (studied as *inertial manifold* by mathematicians, *e.g.* Constantin *et al.* 1989). Our reconstruction analysis indicates that *the dynamics of R Sct evolves on such an inertial manifold, of dimension 4.*

The existence of a 4D inertial manifold thus implies that all dynamical and thermodynamical quantities throughout the star can be expressed in terms of four basic variables. The choice, or the nature of these 4 variables is not unique of course (The variables are defined up to an arbitrary nonlinear transformation). However, in view of our above mentioned work on Cepheids and RR Lyrae stars it seems natural to identify these variables with modal amplitudes, more specifically, with two vibrational (complex) amplitudes. Strong direct support for this role of two vibrational modes comes from the double spiral nature of the fixed points that we uncovered in the maps (*cf.* §4.5). This then leads to the conclusion that *the erratic pulsational behavior is the result of the nonlinear interaction of two (complex) mechanical modes of oscillation.*

In BSKM we have pointed out that the Fourier spectrum for the short data set has noticeable power in the broad vicinity of  $2.5 \times$  the fundamental frequency  $f_0$  peak, even though a peak near  $2.5f_0$  may be less visible in very long data sets (Kolláth 1990). We have also recalled that the period doubling cascade that led to chaos in our W Vir model pulsations originated in a parametric instability, caused precisely by a 5:2 resonance between the fundamental mode of oscillation of the stellar model and an overtone (Moskalik & Buchler 1990). Whether for RV Tau stars this resonance also plays a role needs to be checked with a systematic numerical hydrodynamic modelling survey of RV Tau stars.

## 7. CONCLUSIONS

Chaos theory has had the scientific community excited for over a decade. However, when applications to the real world are considered, it is often found that very little useful information can be gained from such studies. In a recent article Ruelle (1994) has assessed the situation and he concludes that the studies of the solar system have been perhaps the most fruitful application of *Hamiltonian chaos* theory. It is therefore interesting that one of the more fruitful applications of *dissipative chaos* should also occur in Astronomy, this time in variable stars.

The successful reconstruction of the dynamics of R Sct shows that large amplitude irregular stellar variability is no longer a mystery. Our data analysis corroborates the previous theoretical finding (BK87, KB88) that the mechanism for the irregular variability of the Pop. II Cepheids is low-dimensional chaos that arises simply and naturally in the dynamics of the star.

From a physicist's point of view it is interesting that the complicated and relatively violent pulsational behavior of this star takes place in a 4-D phase-space (inertial manifold). We have produced evidence that the observed chaotic behavior has a simple underlying physical model, namely it is the result of the nonlinear interaction of two normal vibrational modes.

The type of analysis that we have presented here opens up the exciting possibility of *nonlinear astro-seismology*. In a way very similar to the study of multi-periodic stars (*e.g.* bump or beat Cepheids, beat RR Lyrae, pulsating white dwarfs,  $\delta$  Scuti stars, *etc.*) the properties of the irregular pulsations can be used to probe the stellar interior and to provide new insights into stellar structure and evolution. While it is clear that more experience is required in the applications of the analysis one can foresee that with a sufficient observing effort one may be able to extract systematically *quantitative information* from irregular variable star lightcurves. This could be in the form of quantities that are still relatively unfamiliar in Astronomy, such as, for example, Lyapunov exponents and fractal dimensions.

The Pop. II Cepheids are as bright as their 10 day Pop. I counterparts and it is conceivable that when we understand them better we may be able to use them as well as standard candles for cosmological purposes.

## Acknowledgments

This research has been supported in part by NSF (AST92-18068 and INT94-15868), a Hungarian OTKA grant (F4352), an RDA grant at UF, the French Ministère pour la Recherche et l'Espace, and RCI grant from IBM through UF.

## References

- Abarbanel, H. D. I., Brown, R., Sidorowich, J. J., Tsimring, L. S. 1993, Rev. Mod. Phys. 65, 1331 [ABST93]  
 Arp, H. C. 1955, AJ 60, 1.  
 Broomhead, D. S. & King, G. P. 1987, Physica D 20, 217  
 Brown, R. 1992, Orthonormal Polynomials As Prediction Functions In Arbitrary Phase-Space Dimensions, Institute for Nonlinear Science Preprint, UC San Diego.  
 Brown, R., Rulkov, N. F. & Tracy, E. R. 1994. Phys. Rev. E 49, 3784.  
 Buchler, J. R. 1990, Ann. NY Acad. Sci. 617, 17  
 Buchler, J. R. 1993, Nonlinear Phenomena in Stellar Variability, IAU Coll. 134, Eds. M. Takeuti & J. R. Buchler (Dordrecht: Kluwer), repr. from 1993, Ap&SS, 210, 1  
 Buchler, J. R., Kolláth, Z. & Serre, T. 1995, in "Waves in Astrophysics", Ann. NY Acad. Sci. (in press)  
 Buchler, J. R. & Kovács, G. 1987, ApJLett. 320, L57-62 [BK87]  
 Buchler, J. R., Serre, T., Kolláth, Z. & Mattei, J. 1995, Phys. Rev. Lett. 74, 842 [BSKM].  
 Casdagli, M., Des Jardins, D., Eubank, S., Farmer J. D., Gibson, J., Hunter, N. & Theiler, J. 1992, in *Applied Chaos*, Ed. J. H. Kim & J. Stinger, 335 (N.Y.: Wiley)  
 Constantin, P., Foias, C. Nicolaenko, B. & Temam, R. 1989. *Integral Manifolds and Inertial Manifolds for Dissipative Partial Differential Equations*, Appl. Math. Sci. 70 (N.Y.: Springer)  
 Gingold, R. A. 1974, ApJ 193, 177  
 Glendenning, P. & Tresser, C. 1985, J. Physique Lett. 46, L347  
 Gouesbet, G. 1991, PR 43A, 5321.  
 Guckenheimer, J. & Holmes, P. 1983, *Nonlinear Oscillations, Dynamical Systems and Bifurcation Theory*, (N.Y.: Springer)  
 Kolláth, Z. 1990, MNRAS 247, 377.  
 Kolláth, Z., Buchler J. R., Serre, T. & Mattei, J. 1995, ApJ (in preparation).  
 Kolláth, Z. & Szeidl, B. 1993, A&A 277, 62.  
 Kovács, G. & Buchler, J. R. 1988, ApJ, 334, 971, [KB88].  
 Kukarkin, B. V. 1975, *Pulsating Stars* (N.Y.: Wiley)  
 Ludendorff, H. 1928, *Handbuch der Astrophysik*, 6, 49  
 Moskalik, P. & Buchler, J. R. 1990, ApJ 355, 590.  
 Ott, E. 1993, *Chaos in Dynamical Systems* (Cambridge: Univ. Press), [O93]  
 Press, W. H., Teukolski, S. A., Vetterling, W. T. & Flannery, B. P. 1992, *Numerical Recipes* (University Press: Cambridge).  
 Reinsch, C. H. 1967, Numerische Mathematik, 10, 177  
 Ruelle, D. 1994, Physics Today, July 24  
 Saitou, M., Takeuti, M. & Tanaka Y. 1989, PASJ 41, 297  
 Scargle, J. D. 1981, ApJS 45, 1  
 Serre, T., Kolláth, Z. & Buchler, J. R. 1995a, A&A (submitted) [SKB]  
 Serre, T., Kolláth, Z. & Buchler, J. R. 1995b, A&A (submitted)

- Thompson, J. M. T. & Stewart, H. B. 1986, *Nonlinear Dynamics and Chaos* (John Wiley and Sons)
- Veldhuizen, T. & Percy, J. R. 1989. *J. AAVSO* 18, 97.
- Weigend, A. S. & Gershenfeld, N. A. 1994, *Time Series Prediction* (Reading: Addison-Wesley) [WG94]